Pediatric Radiology (2020) 50:1907–1920
https://doi.org/10.1007/s00247-020-04678-1

FETAL IMAGING

Imaging of solid congenital abdominal masses: a review of the literature and practical approach to image interpretation

Krista L. Birkemeier[1]

Received: 15 November 2019 / Revised: 27 February 2020 / Accepted: 13 April 2020 / Published online: 19 November 2020

Abstract

Fetal abdominal tumors are rare, usually benign, and cause a great deal of anxiety for expectant parents and the physicians counseling them. In this paper the author reviews the most common fetal abdominal tumors in the liver (hemangioma, mesenchymal hamartoma, hepatoblastoma, metastases) and the kidney (congenital mesoblastic nephroma, Wilms tumor, malignant rhabdoid tumor, and clear cell sarcoma), and suprarenal mass lesions (adrenal neuroblastoma, adrenal hemorrhage, and subdiaphragmatic extralobar pulmonary sequestration). The author describes the imaging approach, imaging appearance and differentiating features of tumors, and differences between fetal and childhood appearances of tumors.

Keywords Abdomen · Adrenal gland · Fetus · Kidney · Liver · Magnetic resonance imaging · Mass · Sequestration

Introduction

Solid abdominal masses in the perinatal period are rare and usually benign. In a review of 44,560 pregnancies, only 8 (0.018%) were solid tumors [1]. The purpose of this article is to discuss the differential diagnosis of solid fetal abdominal tumors, the appearance of the most common diagnoses, and appropriate postnatal imaging (Table 1). This review was approved by the institution's review board.

Prenatal ultrasound (US) is the first-line modality, and fetal MRI is indicated for any fetal abdominal mass suspected on ultrasound because MRI adds information that contributes to the differential diagnosis and management. Fetal MRI is beneficial for its soft-tissue contrast, multi-planar imaging, large field of view, and the utility of T1-W imaging for delineating blood and meconium. Fetal MRI is also less constrained by fetal position, maternal soft-tissue attenuation, gestational age, and oligohydramnios. US imaging remains particularly useful to evaluate Doppler flow and calcifications, and to monitor lesion size and complications over time. For evaluating fetal abdominal masses, a combination of US and MRI is optimal. Often, postnatal imaging is necessary to confirm or further delineate the final diagnosis, provide a postnatal baseline study, and evaluate for metastases.

Liver tumors

Hepatic tumors account for 5% of all perinatal tumors, with hepatic vascular tumors being the most frequent, followed by mesenchymal hamartoma, hepatoblastoma and metastases [2]. There are rare reported cases of perinatal angiosarcoma [2], hepatic adenoma [2–4], focal nodular hyperplasia [2, 5, 6], germ cell tumors, hepatocellular carcinoma and hepatic sarcoma [2]. Liver metastases can occur in utero, most commonly from neuroblastoma. If a primary extrahepatic tumor is not identified in the presence of multifocal liver lesions, consider multifocal infantile hemangioma (although it is less common prenatally) and leukemia.

Prenatally, lesions are detected by US imaging and further evaluated with fetal MRI. Close sonographic follow-up in the prenatal period tracks tumor growth, mass effect that could contribute to pulmonary hypoplasia, gastrointestinal obstruction or vascular compromise, and potential heart failure from vascular shunting. Postnatal multiphase contrast-enhanced MRI or CT confirms peripheral discontinuous nodular enhancement of a hepatic vascular lesion or heterogeneous enhancement of hepatoblastoma or metastases. Hemangiomas

✉ Krista L. Birkemeier
Krista.Birkemeier@bswhealth.org

[1] Department of Radiology, Pediatric Section, Baylor Scott and White Health-Temple, McLane Children's Medical Center, Texas A&M Health Science Center, 2401 S. 31st St., MS-01-W256, Temple, TX 76508, USA

Table 1 Most common fetal abdominal masses based on location

Liver	Kidney	Suprarenal
Hemangioma	Congenital mesoblastic nephroma	Adrenal neuroblastoma
Mesenchymal hamartoma	Wilms tumor	Adrenal hemorrhage
Hepatoblastoma	Malignant rhabdoid tumor	Subdiaphragmatic extralobar pulmonary sequestration
Metastases	Clear cell sarcoma	

can be followed with US imaging to monitor regression, while neoplastic tumors are usually resected.

Hemangioma

Hepatic vascular lesions account for 60.3% of liver tumors diagnosed prenatally and in the first 2 months of age in the pathology literature [2]. Historically there have been many names for vascular liver tumors, including arteriovenous malformation, hemangioendothelioma, cavernous hemangioma, hepatic vascular malformation with associated capillary proliferation, and solitary hemangioma. The confusing nomenclature results in difficulty studying these lesions. In 1982, Mulliken and Glowacki divided vascular lesions into vascular tumors and vascular malformations, and this model was adopted by the International Society for the Study of Vascular Anomalies (ISSVA) in 1996 [7]. In a 2014 update to the ISSVA classification, hepatic hemangiomas were subdivided into infantile hemangiomas and congenital hemangiomas; congenital hemangiomas were further subclassified into rapidly involuting congenital hemangiomas (RICH), non-involuting congenital hemangiomas (NICH) and partially involuting congenital hemangiomas (PICH) [7]. As the name implies, congenital hemangiomas are more commonly detected on fetal imaging, whereas infantile hemangiomas are more commonly detected in infancy.

Congenital hemangiomas are glucose transporter Type 1 (GLUT1) (−) on pathological evaluation, are detected prenatally or soon after birth, are more often a solitary mass, and usually regress within a year or two. They are prenatally identified in the third trimester as a large circumscribed liver tumor. Congenital hemangiomas demonstrate variable echogenicity and are T2-hyperintense but commonly heterogeneous because of areas of necrosis, hemorrhage and calcification. There are sometimes large vessels at the periphery of the lesion and vascular shunting as evidenced by large arteries and draining veins, small caliber of the aorta distal to the liver, and cardiomegaly [8–10] (Fig. 1). Occasionally they present as a homogeneous liver mass (Fig. 2). Hydrops is a potential complication. Congenital hemangiomas can be complicated by transient consumptive coagulopathy [10].

Infantile hemangiomas are GLUT1 (+) on pathological evaluation, are more often diagnosed in the first few months of age, are more often multiple or diffuse but can be solitary, and typically grow during the first year of age and then regress over 1–8 years. Infantile hemangiomas have an interesting association with hypothyroidism, which can be profound; they sometimes express Type 3 iodothyronine, which degrades thyroid hormone, so thyroid supplementation might be necessary until the lesion resolves or is resected [11]. Hypothyroidism can also contribute to heart failure in these children [10]. Infantile hemangioma is also more highly associated with skin hemangiomas than congenital hemangioma. Infantile hemangioma typically presents as smaller multifocal or diffuse tumors of variable echogenicity and hyperintense T2-W signal that sometimes nearly replaces the liver parenchyma on imaging compared to the large solitary heterogeneous congenital hemangioma [8, 9] (Fig. 3; Table 2).

Postnatal contrast-enhanced multiphase imaging is recommended to confirm a vascular tumor by demonstrating the typical arterial-phase discontinuous nodular enhancement with centripetal fill-in over time. MR is favored for postnatal imaging because of its lack of ionizing radiation. Large tumors commonly have central necrosis, which does not enhance (Fig. 2). If there is rapid growth or if the enhancement pattern is not typical, the lesion should undergo biopsy. Commonly, postnatal imaging confirms the diagnosis and asymptomatic lesions are followed with US imaging to document regression. Symptomatic lesions, usually with vascular shunting or mass effect, are treated with steroids to hasten involution or anti-angiogenic drugs; when symptomatic lesions are refractory to medical management, they are treated with embolization, tumor resection or liver transplantation. GLUT1 (+) infantile hemangiomas more reliably respond to medical management, whereas there is no clear effect on GLUT 1 (−) congenital hemangiomas [10, 12].

Mesenchymal hamartoma

Mesenchymal hamartomas account for 23.3% of liver tumors diagnosed prenatally through the first 2 months of age in the pathology literature [2]. The etiology is not established,

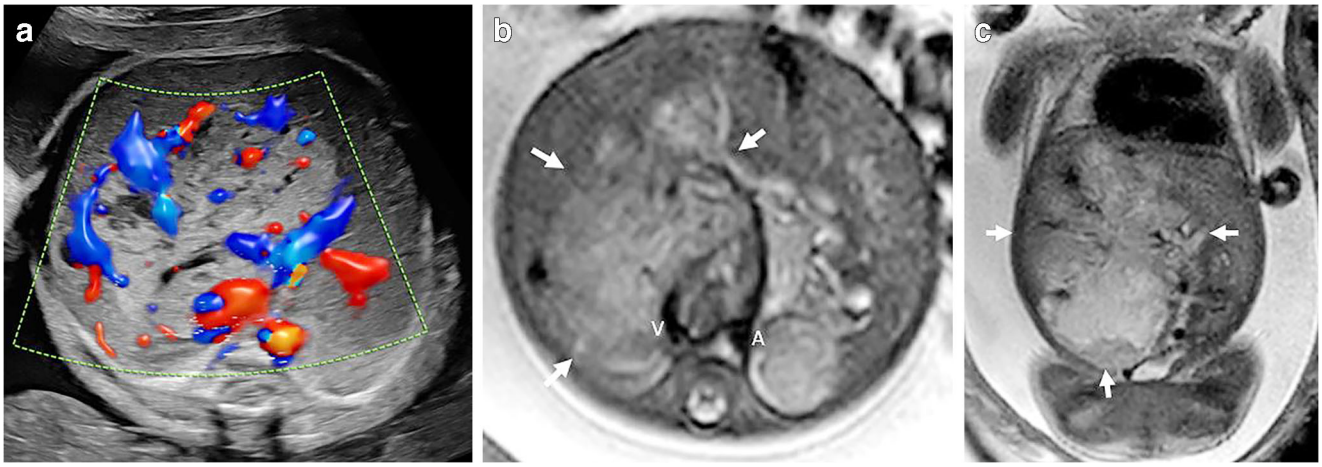

Fig. 1 Congenital hemangioma. Prenatal imaging at 29 weeks of gestation of a congenital hemangioma, confirmed on autopsy. The baby was born at 30 4/7 weeks and died of refractory high-output cardiac failure. **a** Transverse Doppler US imaging demonstrates a heterogeneous hypervascular liver mass with abundant Doppler flow. **b** Axial T2-W half-Fourier acquisition single-shot turbo spin-echo (HASTE) MR image demonstrates a heterogeneous mass (*arrows*) with large peripheral vessels, large-caliber hepatic artery arising from the aorta (*A*) and large vein draining to the inferior vena cava (*V*). **c** Coronal T2-W HASTE MR image shows the hypervascular mass (*arrows*) in addition to cardiomegaly, indicating heart failure secondary to shunting. Images courtesy of Dr. Chris Cassady

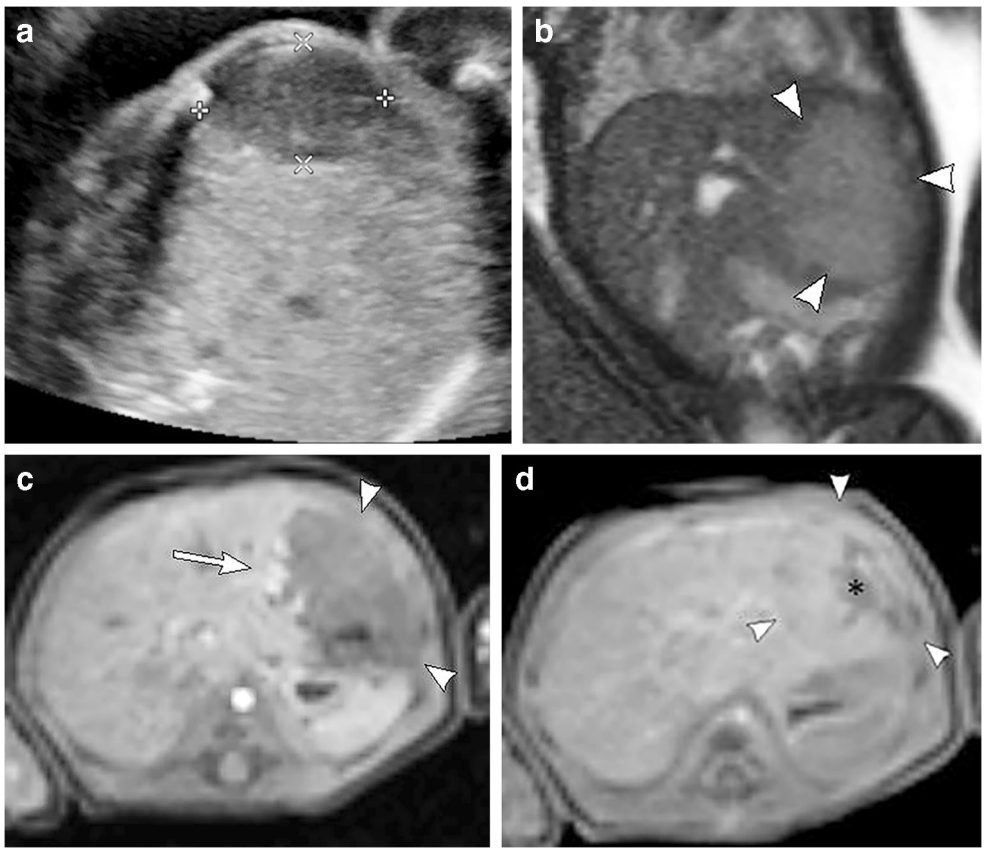

Fig. 2 Homogeneous hemangioma. Prenatal and postnatal imaging of an atypically homogeneous congenital hemangioma in a male. **a** Transverse US image at 31 weeks of gestation demonstrates a well-circumscribed, more homogeneous hypoechoic mass (*calipers*) than is typical for congenital hemangioma. **b** Coronal TrueFISP (true fast imaging with steady-state precession) MR image at 33 weeks of gestation confirms the intrahepatic mass (*arrowheads*) and reveals no other findings. **c** Postnatal axial contrast-enhanced arterial-phase T1-W fat-saturated MRI of the boy's abdomen at 4 days of age confirms that the mass (*arrowheads*) is a hemangioma with characteristic peripheral discontinuous nodular enhancement (*arrow*). **d** There is centripetal fill-in over time, and on delayed axial post-contrast T1-W MRI the mass (*arrowheads*) demonstrates an area of nonenhancement (*asterisk*) from necrosis that is common in congenital hemangioma

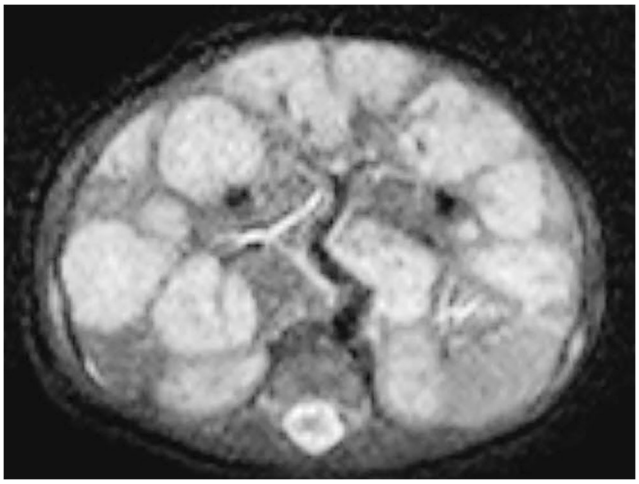

Fig. 3 Infantile hemangioma. MRI in a 5-week-old girl who presented with heart failure at 4 weeks of age and multiple masses on US imaging. Postnatal axial T2-W MR image demonstrates multiple T2-hyperintense hepatic lesions with vascular flow voids throughout the liver, typical of infantile hemangiomas

although they might represent a type of ductal plate malformation, a hamartoma, or the result of toxic or ischemic injury [13].

Mesenchymal hamartomas are multilocular cystic and solid lesions typically diagnosed prenatally in the second and third trimesters (Fig. 4). On imaging there are commonly several septations and nodules, and sometimes hemorrhage or debris within the cysts. Calcifications or a large solid angiomatous component might be present. They are pedunculated in 20% of cases, which can cause difficulty in determining hepatic origin of the mass. Other cystic lesions in the right upper quadrant should also be considered if the mass is predominantly cystic and pedunculated [14]. Other differential considerations include hemangioma or hepatoblastoma with a cystic component, but typically those tumors are largely solid compared to mesenchymal hamartoma, which is largely cystic.

Lesion size is variable, and complications are related to mass effect. Polyhydramnios, hydrops and pulmonary hypoplasia have been reported, with 29% mortality for lesions diagnosed in utero [15]. For this reason, close prenatal follow-up to monitor size is recommended, and some advocate aspiration of large cysts for temporary relief of mass effect. Most lesions are completely resected postnatally because there have been rare case reports of undifferentiated embryonal sarcoma arising in partially resected lesions [14]. There have been reports of spontaneous regression, as well (Fig. 5).

Hepatoblastoma

Hepatoblastomas account for 16.5% of liver tumors diagnosed prenatally through the first 2 months of age in the pathology literature [2]. Of all pediatric hepatoblastomas, only 10% are diagnosed in the perinatal period [2]. Hepatoblastoma is associated with Beckwith–Wiedemann syndrome and familial adenomatous polyposis [16, 17].

On prenatal imaging, hepatoblastoma is identified in the late third trimester as a large heterogeneous mass. It is usually solitary but can be multifocal. It is typically a hyperechoic solid mass on US imaging with increased vascularity and is predominantly T2-hyperintense and T1-hypointense (Fig. 6). There might be areas of heterogeneity from hemorrhage, necrosis or calcification. As with any abdominal mass lesion, there is sometimes mass effect with potential pulmonary hypoplasia, compression of venous structures, and hydrops.

While childhood cases of hepatoblastoma metastasize to the lung, fetal circulation presumably accounts for sparing of the lungs in prenatal cases. However, it can metastasize to the brain, bone and placenta.

Other liver tumors such as hemangioma, metastasis and mesenchymal hamartoma with a large solid component are in the differential diagnosis. Interestingly, while nearly all childhood hepatoblastomas result in a markedly elevated alpha-fetoprotein (AFP) level, only about half of fetal hepatoblastomas do, so this lab test does not rule out hepatoblastoma. Additionally, AFP is elevated in 14% of fetal hemangiomas and rarely in mesenchymal hamartoma [2].

Table 2 Comparison of common characteristics of congenital hemangioma versus infantile hemangioma

	Congenital	Infantile
Diagnosis	Prenatal 3rd trimester	Postnatal weeks to months
Postnatal course	Rapidly involuting congenital hemangioma (RICH) involutes over a year Non-involuting congenital hemangioma (NICH) stabilizes or grows Partially involuting congenital hemangioma (PICH) partially involutes	Grows first year then involutes
Glucose transporter (GLUT) 1 reactivity	(−)	(+)
Appearance	Large solitary mass	Multifocal or diffuse
Associations	Low association with skin hemangiomas	Strong association with skin hemangiomas and hypothyroidism

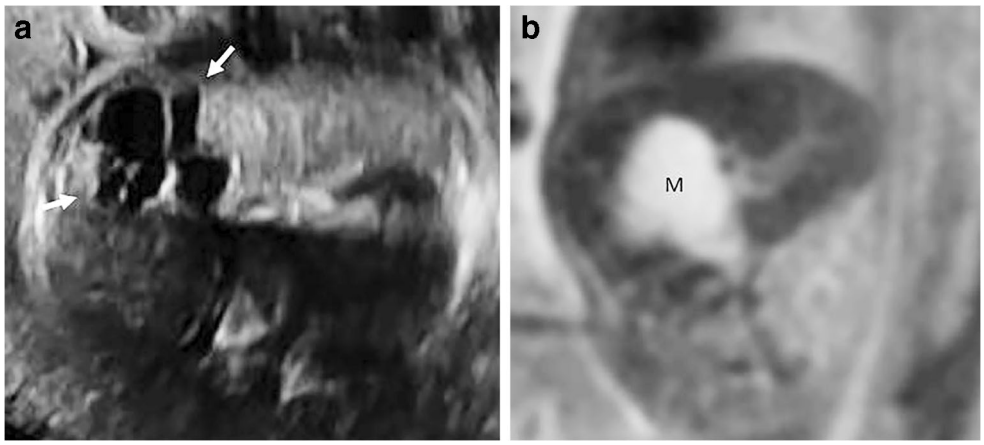

Fig. 4 Mesenchymal hamartoma of the liver on prenatal imaging at 26 weeks of gestation. **a** Transverse US image demonstrates a multilocular cystic liver mass (*arrows*). **b** Sagittal T2-W MR image confirms a hyperintense cystic lesion (*M*) with multiple septations. Images courtesy of Dr. Beth Kline-Fath

Prenatal follow-up evaluates for tumor growth and for development of complications. Postnatally, contrast-enhanced imaging and staging should be performed. Postnatal heterogeneous contrast-enhancement pattern, and therefore lack of hemangioma-specific enhancement, and other aggressive features such as rapid growth or metastases are helpful in diagnosing hepatoblastoma. With modern treatment, congenital hepatoblastoma outcomes are similar to those in childhood hepatoblastoma, with a 3-year survival of 86% [18].

Renal tumors

Solid renal tumors in the fetus and neonate are quite rare and account for 5% of all perinatal tumors [19]. In the perinatal period, congenital mesoblastic nephroma is most common, followed by Wilms tumor, malignant rhabdoid tumor of the kidney, and finally clear cell sarcoma of the kidney. This differs from tumors in the first year after birth, when Wilms tumor is more common than mesoblastic nephroma. There are rare reported cases of multilocular cystic renal tumor (cystic nephroma and cystic partially differentiated nephroblastoma), ossifying renal tumor of infancy, angiomyolipoma (with tuberous sclerosis complex) and metanephric stromal tumor [19–21].

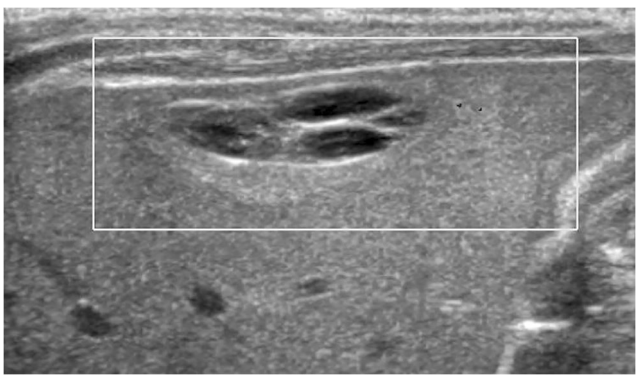

Fig. 5 Resolving mesenchymal hamartoma. Postnatal US image in an 8-week-old boy to follow up a cystic liver mass seen on prenatal imaging at about 6 months of gestation (prenatal imaging not available). US image demonstrates a complex multilocular cystic lesion with no significant Doppler flow. It resolved on follow-up imaging 4 weeks after this image (not shown) and was presumed to be a mesenchymal hamartoma

While US imaging is used first to diagnose a prenatal renal mass, there is considerable overlap in the sonographic appearance of renal tumors, so a final diagnosis is not possible by US imaging. The soft-tissue contrast of MRI is useful to further confirm renal origin, exclude metastases or contralateral lesions, and better define the extent of the lesion [22]. Based on patient age, congenital mesoblastic nephroma is the most likely fetal tumor, with Wilms, rhabdoid, and clear cell sarcoma in the differential diagnosis. MRI findings might cause one to re-order that differential diagnosis. If there were contralateral renal lesions or venous invasion, Wilms would be at the top of the differential diagnosis, followed by rhabdoid tumor. If there were a brain tumor, rhabdoid tumor would be at the top of the differential diagnosis. If there were distant metastases, rhabdoid tumor would be most likely and congenital mesoblastic nephroma least likely.

Prenatally, close follow-up is important to look for polyhydramnios and complications related to mass effect such as cardiovascular compromise, hydrops and pulmonary hypoplasia. These fetal complications, rather than tumor malignancy, are the greatest cause of morbidity and mortality. This is especially true for congenital mesoblastic nephroma, where polyhydramnios is the presenting sign twice as often compared to other renal tumors [19]. Polyhydramnios with fetal renal tumors might be caused by increased perfusion resulting in hyperfiltration and excessive urine production. There might also be a component of gastrointestinal obstruction. In a multicenter study including 26 congenital mesoblastic nephromas and 2 Wilms tumors diagnosed prenatally, 39% had polyhydramnios, 2 fetuses had hydrops, and 1 fetus died. Nearly half of the fetuses with renal tumors were born premature [23].

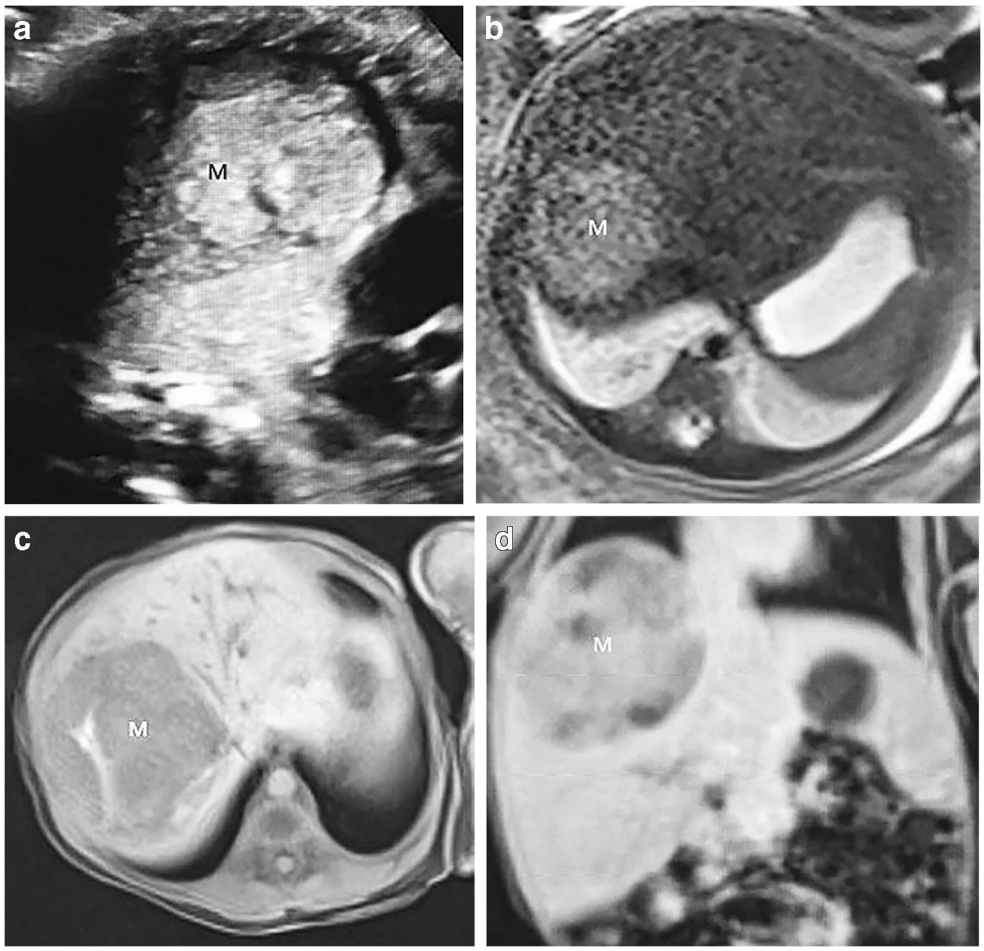

Fig. 6 Hepatoblastoma. Prenatal and postnatal congenital hepatoblastoma in a girl diagnosed postnatally with Beckwith–Wiedemann syndrome. **a** Transverse fetal US image at 37 2/7 weeks of gestation demonstrates a heterogeneous hyperechoic mass (*M*) in the liver. **b** Fetal axial T2-W MRI confirms a heterogeneous hepatic mass (*M*) that measures 3.2×3.3 cm. No metastases were seen. **c** Postnatal axial T1-W fat-saturated MRI arterial-phase imaging 7 days after prenatal imaging demonstrates central arterial enhancement in the mass (*M*). **d** Postnatal contrast-enhanced venous-phase coronal T1-W fat-saturated MRI demonstrates a heterogeneously enhancing mass (*M*). It measured 5.0×5.3 postnatally, significantly increased in size. Images courtesy of Dr. Rachelle Goldfisher

Vaginal delivery is safe in uncomplicated cases. Caesarean section is advisable for large masses, fetal distress or risk of tumor rupture, though there is no established guideline regarding how big is too big [23]. The baby should be delivered at a tertiary care center with a multidisciplinary team. Postnatally, staging is recommended with chest CT and either MR or CT of the abdomen. Nephrectomy should be performed within days to weeks because pathology rather than imaging is diagnostic. Immediate postnatal complications include hypertension (22%), respiratory distress (30%) and hemodynamic instability (11%) [23]. Hypercalcemia is also reported [19, 23].

Congenital mesoblastic nephroma

Congenital mesoblastic nephroma accounts for 66% of renal tumors diagnosed prenatally through the first 2 months of age based on pathology literature [19] and comprised 54% of renal tumors diagnosed in the first month after birth in a study of infants [24]. It is generally considered a benign tumor of fetal and early postnatal infants that is curable with resection; however, there are reported cases of metastases (2%) to the lung, brain, liver, heart and bone, so it is really best classified as a mesenchymal tumor with low malignant potential [19, 25, 26]. Perinatal morbidity and mortality are caused by associated polyhydramnios, mass effect resulting in pulmonary hypoplasia and circulatory compromise, respiratory distress, fetal hypertension, hypercalcemia and preterm labor, so 5% of patients with congenital mesoblastic nephroma die before or shortly after birth [19, 25].

On imaging, congenital mesoblastic nephroma is usually a large mass comprising half or more of the kidney, located near the hilum, and sometimes involving part or all of the renal sinus [22, 25]. Based on case reports, congenital mesoblastic nephroma on US imaging is usually a homogeneous mass that is not encapsulated and blends in with the renal parenchyma. However, sonographic variants including mild heterogeneity, a hypo- or hyperechoic rim, cysts and calcifications have been described [23, 25]. There is typically some degree of internal vascularity [22]. Given the variety of appearances and overlap with other tumors, especially Wilms tumor, sonography is not diagnostic of the type of tumor [23]. On MRI the signal is isointense to renal parenchyma (Fig. 7).

Survival among treated perinatal patients is 84%, which is lower than the survival rate for congenital mesoblastic nephroma in older infants (96%), likely because prenatal conditions (polyhydramnios, hydrops, hypertension, pulmonary

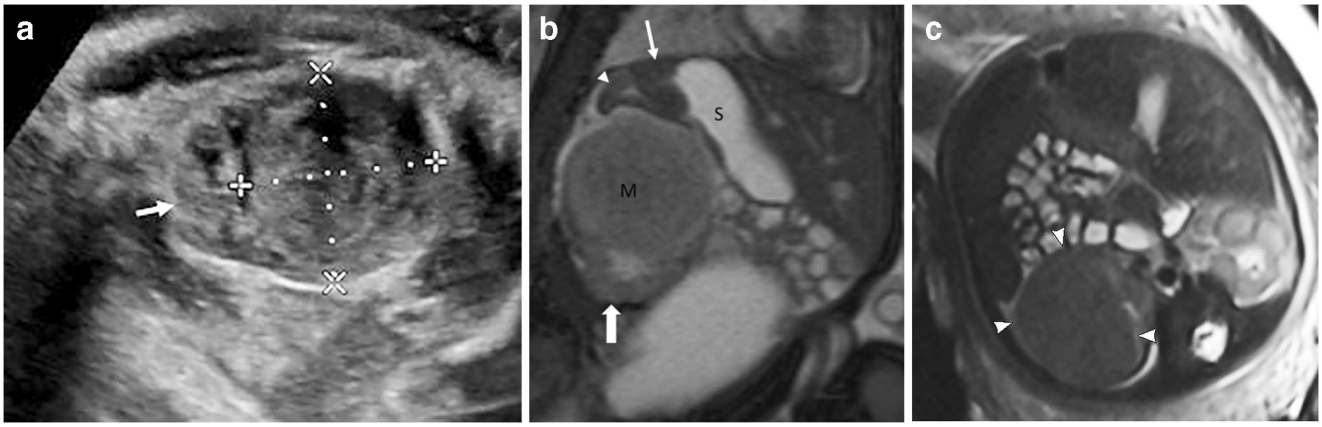

Fig. 7 Congenital mesoblastic nephroma. Prenatal imaging of a fetus referred for left renal tumor identified in the third trimester. **a** Prenatal longitudinal US image at 35 weeks of gestation demonstrates a mildly heterogeneous left renal mass (*calipers*) of similar echogenicity to the rim of normal renal cortex superiorly (*arrow*). **b** Sagittal TrueFISP (true fast imaging with steady-state precession) T2-W MR image demonstrates the renal mass (*M*) separate from the adrenal gland (*arrowhead*), spleen (*thin arrow*) and stomach (*S*). It replaces more than half the kidney (*thick arrow*), compresses the hilum, and demonstrates signal isointense to the renal cortex and blends into the cortex. **c** Axial half-Fourier acquisition single-shot turbo spin-echo (HASTE) T2-W MRI demonstrates the left renal mass (*arrowheads*), which is isointense to the normal contralateral renal cortex

hypoplasia, heart failure) affect morbidity and mortality and decisions regarding surgical treatment [19, 24]. Nephrectomy is the treatment of choice because there is increased likelihood of local recurrence with positive margins after partial nephrectomy [26]. Recurrence rate is 5% [19, 25].

Wilms tumor

Wilms tumor accounts for 20% of renal tumors diagnosed prenatally through the first 2 months of age based on pathology literature [19]. On imaging, Wilms tumor is a large solid infiltrating tumor that sometimes has areas of hemorrhage, necrosis and rarely calcification. It has been described as encapsulated. Some authors favor a Wilms diagnosis if there appears to be a capsule or increased heterogeneity of tumor on prenatal imaging [27], but there is overlap in the imaging appearance with other tumors. Wilms tumor is known to invade the renal vein and inferior vena cava.

Because bilateral tumors and nephrogenic rests might be present [28], this is a renal tumor for which MRI is particularly useful to analyze the contralateral kidney, to analyze the ipsilateral kidney for vascular invasion, and to look for metastases.

Prognosis is good, with 91% survival with treatment in perinatally diagnosed cases [19], which is similar to those diagnosed in the first 7 months of age, who have a 93% 5-year overall survival [24].

Malignant rhabdoid tumor of the kidney

Malignant rhabdoid tumor of the kidney accounts for 11% of renal tumors diagnosed prenatally through the first 2 months of age based on pathology literature [19]. It is locally aggressive with infiltration and invasion of the capsule and vessels. Metastases are present at diagnosis in about half of cases [19, 25]. There are simultaneous brain tumors, particularly medulloblastomas and primitive neuroectodermal tumors, in 26% of cases [19], and the brain should be scrutinized in fetuses with renal tumors.

A case report of a prenatal malignant rhabdoid tumor of the kidney detected just prior to delivery describes a heterogeneous large mass, which on postnatal MRI demonstrated heterogeneous enhancement and areas of necrosis and hemorrhage [29]. Because it is an aggressive tumor, it is often large, with vascular invasion and indistinct margins. Malignant rhabdoid tumor of the kidney resembles Wilms tumor except that curvilinear calcifications are more likely in malignant rhabdoid tumor and subcapsular hemorrhagic fluid collections are described as characteristic [30].

Prognosis is poor, with only 8.7% survival with treatment in a small number of prenatally diagnosed cases. Presence of metastases nearly ensures fatality [19]. The 5-year survival for children diagnosed in their first 7 months of age remains bleak at 16% [24].

Clear cell sarcoma of the kidney

Clear cell sarcoma of the kidney accounts for 2.5% of renal tumors diagnosed prenatally through the first 2 months after birth based on pathology literature [19]. It is referred to as the "bone metastasizing tumor," though it also metastasizes to lymph nodes, lung and liver, and less commonly to soft tissue, brain, skin, colon and the contralateral kidney [31]. It presents as a large centrally located, well-circumscribed mass.

Heterogeneity from cysts, necrosis and hemorrhage might occur. Rarely it extends into the renal vein [31].

In children younger than 3 months, clear cell sarcoma of the kidney tends to be low-stage [24], with better prognosis in prenatally than postnatally diagnosed tumors [32], and there is 86% survival with treatment in the rare fetal/perinatal cases [19].

Suprarenal mass lesions

The differential diagnosis for suprarenal mass lesions includes adrenal hemorrhage, neuroblastoma and subdiaphragmatic extralobar pulmonary sequestration. Adrenal hemorrhage and neuroblastoma tend to be on the right side and diagnosed in the third trimester, whereas sequestration tends to be on the left side and diagnosed in the second trimester. Imaging evaluation of echogenicity, vascularity, cysts, MR signal, adrenal involvement, spine involvement and diaphragmatic defect are all key findings to narrow the differential diagnosis (Table 3).

There have been case reports of other rare lesions including adrenal cortical adenoma [33, 34] and adrenal carcinoma [35]. Neuroblastoma in situ describes a microscopic focus of malignant neuroblastoma in a macroscopic cyst visible on imaging. Rarely, isolated adrenal cysts have been described, and there have been cases of a simple-appearing perinatal adrenal cyst evolving to a complex cyst and then a complex mass, and later confirmed as neuroblastoma [36, 37].

Neuroblastoma

Neuroblastoma is a tumor of postganglionic sympathetic neurons found in young children. Neuroblastoma detected in utero or in the first month of age is rare, but it is the most common perinatal malignancy. It most commonly arises in the adrenal gland (74.5%), though non-adrenal retroperitoneal (11.8%) and extra-abdominal locations have been reported prenatally [38, 39]. Perinatal neuroblastoma tends to be less aggressive than childhood neuroblastoma, with favorable histology in 86% [38]. Perinatal neuroblastoma demonstrates elevated urine catecholamines in a little more than half of cases based on a large retrospective study in the pathology literature [38]. Conversely, reports regarding neuroblastoma in children typically cite 90–95% of cases with elevated urine catecholamines.

Prenatally, neuroblastoma is typically identified by US imaging in the third trimester as a cystic, mixed cystic and solid, or heterogeneous solid suprarenal mass (Figs. 8 and 9). There is a slight predilection for the right side in larger studies, with neuroblastoma occurring on the right about 60% of the time [40–42]. Solid components often have Doppler flow, and the septa in cystic neuroblastomas might show Doppler flow. Calcifications are sometimes present but are not as common in perinatal neuroblastoma as in childhood neuroblastoma. On fetal MRI, neuroblastoma demonstrates heterogeneous intermediate signal intensity that is less T2-hyperintense than the lung [43].

Prenatal MRI is useful to confirm adrenal location, exclude spine involvement and evaluate for metastases. In a multicenter review of suprarenal masses, MRI was a useful adjunct to US to correctly diagnose cases that were equivocal on US and to identify liver metastases [43].

MRI might not add much to characterizing the primary lesion for the cystic neuroblastoma subtype. Because cystic neuroblastomas can have superimposed hemorrhage, presence of hemorrhagic MR signal could be from neuroblastoma with tumoral hemorrhage or from adrenal hemorrhage without tumor. Follow-up over time is useful in those cystic neuroblastoma cases. For cystic perinatal neuroblastoma, about 1/3 decrease in size with increased complexity, 1/3 do not change in size but demonstrate increased heterogeneity, and 1/3 demonstrate no change in size or appearance on follow-up imaging [42].

In fetuses and neonates, half or more neuroblastomas are the cystic subtype, which is thought to represent neuroblastoma in situ [38, 42]. Cystic neuroblastoma is distinct in that it is less likely to demonstrate elevated urine catecholemines than solid tumors, has better survival, is a lower stage at diagnosis, and is less likely to metastasize [41, 42]. Survival for children diagnosed before birth (88%) is better than for those diagnosed postnatally (64%), and there is improved survival for cystic neuroblastoma (92%) compared to non-cystic neuroblastoma (70%) [38]. Spontaneous regression of neuroblastoma has been documented in mass-screening studies in infants [44].

Table 3 Comparative features of suprarenal masses

Neuroblastoma	Adrenal hemorrhage	Sequestration
Right>left	Right>left	Left>right
3rd trimester	3rd trimester	2nd trimester
Heterogeneous, cysts, variable echogenicity, intermediate to high T2-W signal < lung	Variable echogenicity and signal, early hyperechoic, T1-W hyperintense	Homogeneous, hyperechoic, high T2-W signal > lung
Adrenal/spine involvement	Changes over time, decreasing in size and echogenicity	Associated diaphragm defect

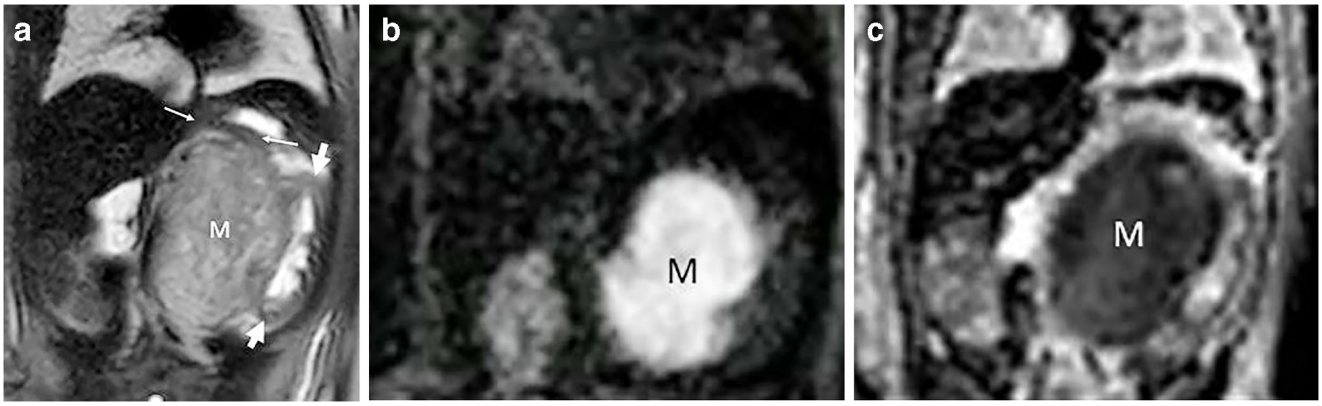

Fig. 8 Neuroblastoma. Prenatal MRI in a 37-week fetus with a large solid left-upper-quadrant congenital neuroblastoma. **a** Coronal T2-W single-shot fast spin-echo (SSFSE) MRI demonstrates a large heterogeneous solid mass (*M*) arising from the left adrenal gland (*thin arrows*) that displaces the kidney (*thick arrows*). It shows intermediate signal and hypointensity relative to lung. **b** The mass (*M*) is hyperintense on coronal diffusion-weighted MR imaging. **c** Restricted diffusion is confirmed with low signal in the mass (*M*) on the apparent diffusion coefficient map, as expected for a small round blue cell tumor. Images courtesy of Dr. Chris Cassady

The liver is the main site of metastasis for neuroblastoma in this age group (Fig. 9), followed by bone marrow, skin, lungs, lymph nodes, placenta and pancreas [38]. Solid tumors are more likely to metastasize than cystic tumors [42, 43, 45]. Children with intraspinal extension have increased risk for irreversible paralysis regardless of treatment [38].

Complications include hemoperitoneum from tumor rupture, respiratory distress caused by metastatic hepatomegaly with lung compression, compression of lungs secondary to primary tumor size, and stillbirth. Cardiac malformations have been associated with neuroblastoma in 10–20% of cases, so cardiac screening is warranted [38].

Adrenal hemorrhage

Adrenal hemorrhage might occur secondary to perinatal distress such as hypoxia, septicemia, birth trauma or bleeding disorder, but it has also been observed in the absence of a known physiological stressor and in cases of Beckwith–Wiedemann syndrome. Adrenal hemorrhage is more common in large babies. The incidence is approximately 0.28–0.55% and it can be asymptomatic [46, 47]. It has been proposed that compression during birth causes vascular rupture, or that transient hypotension or hypoxia might cause hemorrhage [48]. The right adrenal vein is relatively shorter than the left and has been proposed as a reason for preferential hemorrhage; it occurs on the right more often than left and is bilateral in 5–10% [41, 48].

On imaging, hemorrhage is either adreniform or mass-like. It is acutely echogenic, then becomes more hypoechoic and anechoic as it liquefies. As it resolves it might resorb and disappear or there might be calcification within months [41]. The signal on MRI is variable on T2-W imaging, hyperintense on T1-W imaging, and markedly hypointense on echoplanar imaging and gradient echo imaging because of hemosiderin (Fig. 10).

Differentiating adrenal hemorrhage from cystic neuroblastoma can be challenging. They are both more commonly right-side suprarenal tumors identified in the third trimester, though they can occur on either side. In a study analyzing multimodality appearance of 16 congenital cystic neuroblastomas and 14 hemorrhagic pseudocysts, there was no

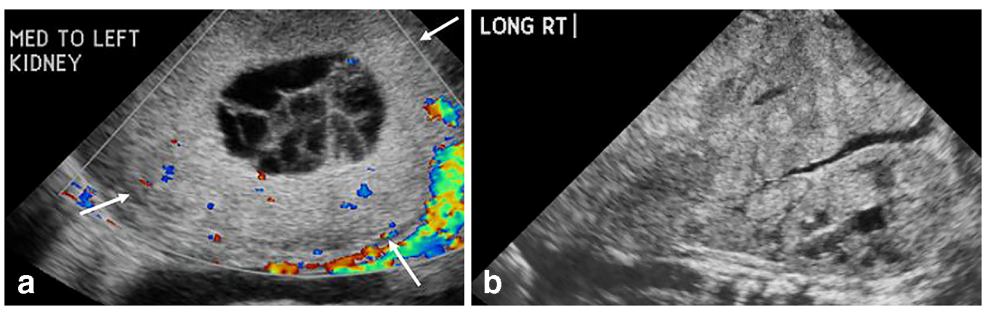

Fig. 9 Neuroblastoma with metastases. Postnatal imaging of a newborn girl at 0 days of age with placental metastases at delivery, which prompted this postnatal abdominal US imaging; longitudinal images shown. **a** Left upper quadrant suprarenal mass replaces the adrenal gland. It is peripherally solid and echogenic with Doppler flow (*arrows*) and central complex cystic component. **b** There are innumerable hyperechoic metastases in the liver

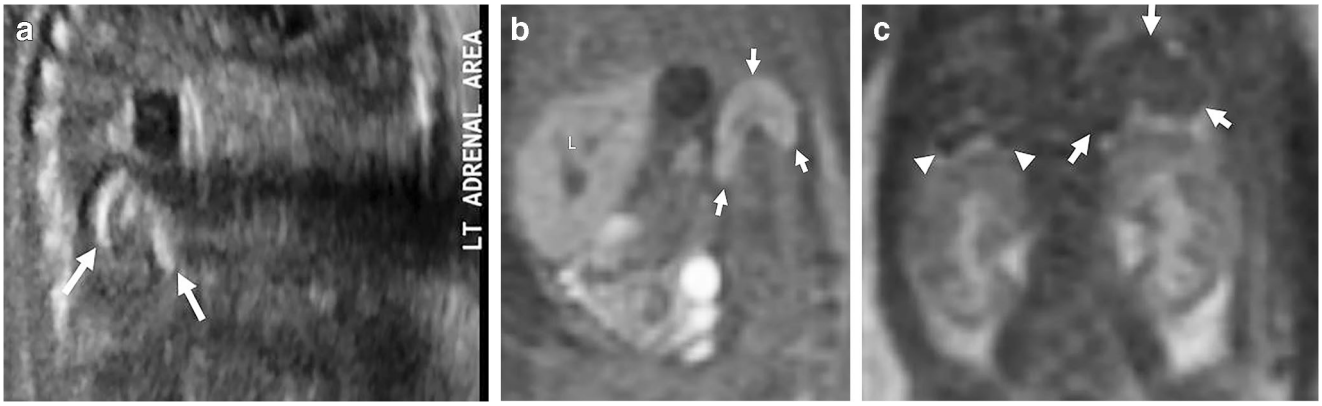

Fig. 10 Adrenal hemorrhage. Prenatal imaging in a 29-week fetus with a cloacal malformation, anhydramnios, pulmonary hypoplasia and adrenal hemorrhage. **a** Longitudinal ultrasound demonstrates adreniform hyperechogenicity above the kidney (*arrows*). **b** Sagittal T1-W MRI demonstrates adreniform hyperintense signal of hemorrhage (*arrows*). **c** Coronal T2-W half-Fourier acquisition single-shot turbo spin-echo (HASTE) MRI demonstrates an enlarged heterogeneous and predominantly hypointense left adrenal gland (*arrows*) in comparison to the normal right adrenal gland (*arrowheads*)

significant difference in the presence of a solid-appearing component, septa, enhancement, or presence of echoes in fluid; however, tiny calcifications (n=3) and vascular flow in the wall (n=3) were seen only in neuroblastomas. Follow-up over 25–150 days revealed that all the adrenal hemorrhages resolved with or without small calcifications. Neuroblastomas that were not initially resected decreased in size over 45–90 days and became more complex but did not resolve. It is hypothesized that the cystic component resorbs and solid component increases over time [41]. Prenatal MRI to look for signal characteristics of neuroblastoma versus hemorrhage, spinal involvement, or metastases should be performed prenatally, and sonographic follow-up should be performed postnatally.

Subdiaphragmatic extralobar bronchopulmonary sequestration

Bronchopulmonary sequestrations are composed of dysplastic lung tissue with systemic arterial supply and lack of airway communication. They are divided into intralobar and extralobar depending on pulmonary versus systemic drainage and relationship to normal lung pleura. They are relatively common in terms of fetal lung lesions. Extralobar sequestrations are more common than intralobar sequestrations when detected prenatally [49]. Those located outside the chest are extralobar and are relatively uncommon, with up to 15% of sequestrations being intra-abdominal, up to 5% trans-diaphragmatic, and up to 2.8% intra-diaphragmatic [49, 50]. Arterial supply for abdominal lesions is usually from the aorta or celiac axis. Regardless of location, a sequestration–congenital pulmonary airway malformation (CPAM) hybrid lesion can occur. Subdiaphragmatic extralobar bronchopulmonary sequestration is detected in the second trimester and its growth plateaus at about 26 weeks of gestation, similar to CPAM, and then it becomes smaller and more isoechoic [49].

Sequestrations are usually homogeneous unless they contain cysts. They are more hyperechoic than lung on US imaging, and the T2 hyperintensity is between that of lung and amniotic fluid. A feeding systemic artery also supports this diagnosis. They are associated with diaphragmatic defects (Fig. 11) [43, 51]. Pulmonary sequestration is associated with congenital diaphragmatic hernia, diaphragm eventration, diaphragm paralysis, pericardial defects, foregut malformations, ectopic pancreas, vertebral anomalies and pectus excavatum [50, 51].

Outcome data specifically for subdiaphragmatic extralobar bronchopulmonary sequestration are limited because these sequestrations are rare and are only included as a small subset in large studies of pulmonary sequestrations. Many subdiaphragmatic extralobar bronchopulmonary sequestrations are resected for risk of infection or malignant degeneration, and some are resected for symptoms related to mass effect or infection. However, some authors advocate imaging follow-up without surgery in asymptomatic children, and there have been case reports of spontaneous resolution [52–54]. Most extralobar sequestrations do not get infected unless there is a communication with the gastrointestinal system. There are only rare case reports of malignancy arising in an extralobar sequestration [54].

It is important to differentiate neuroblastoma from subdiaphragmatic extralobar bronchopulmonary sequestration, particularly because a sequestration might not require resection. Prenatally, neuroblastoma tends to be on the right side, shows intermediate signal on T2-W imaging and less intensity than the lung, usually involves the adrenal gland or spine, and is not associated with diaphragmatic defects.

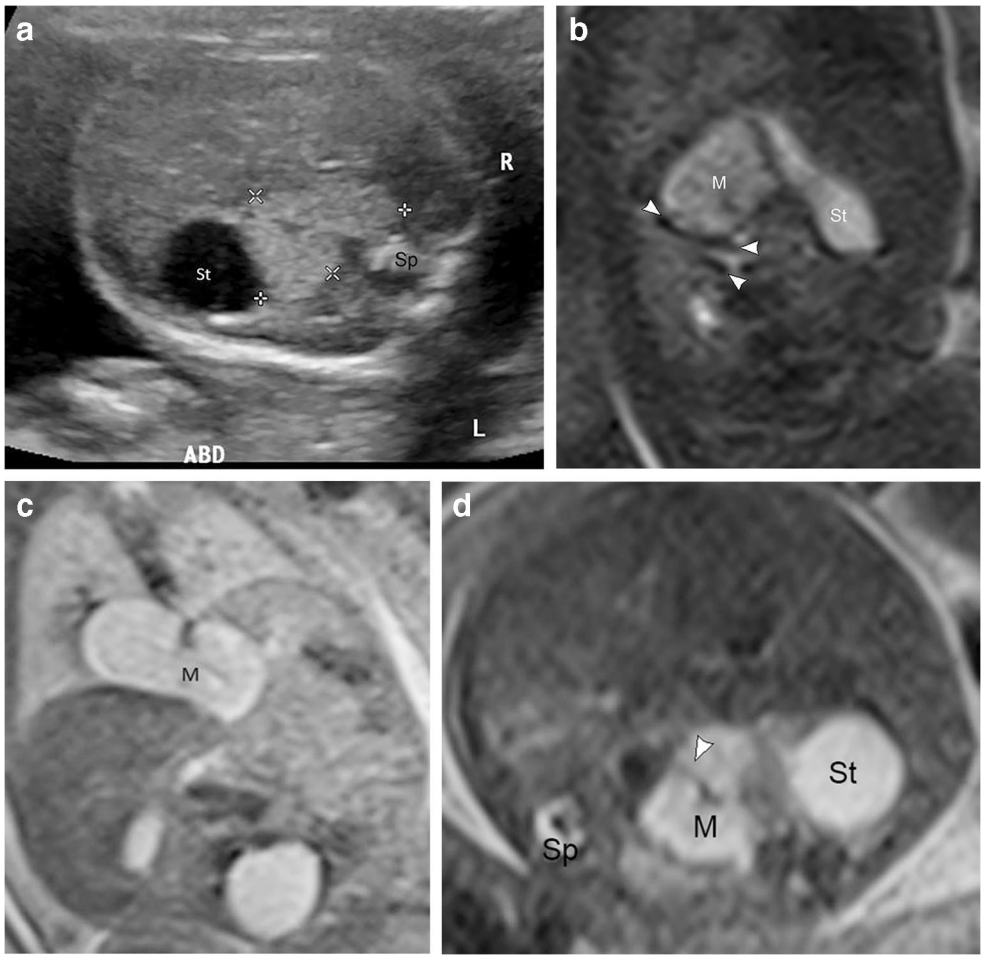

Fig. 11 Bronchopulmonary sequestrations. Prenatal imaging of a subdiaphragmatic extralobar pulmonary sequestration identified in the second trimester. **a** Axial US image at 20 weeks of gestation demonstrates a hyperechoic mass (*calipers*) medial to the stomach (*St*) in the left upper quadrant that extends across the midline spine (*Sp*). **b** Sagittal half-Fourier acquisition single-shot turbo spin-echo (HASTE) image from a fetal MRI study at 27 2/7 weeks of gestation shows that the mass (*M*) is separate from the adrenal gland (*arrowheads*) and posterior to the stomach (*St*). **c** Coronal HASTE MRI demonstrates the mass (*M*) in the left upper quadrant of the abdomen, extending through a diaphragm defect into the right lower chest. The mass is hyperintense relative to lung but less intense than amniotic fluid and urine in the bladder. **d** Axial HASTE MRI demonstrates the flow void of the systemic vessel (*arrowhead*) supplying the mass (*M*). The spine (*Sp*) and stomach (*St*) are labeled for orientation

Subdiaphragmatic extralobar bronchopulmonary sequestration is more often on the left side, demonstrates homogeneous hyperintense T2-W signal between lung and amniotic fluid, is separate from the adrenal gland and spine, and is sometimes associated with a diaphragmatic defect [40, 43].

Other tumors and mimics

Teratoma

Teratoma is a heterogeneous mass with solid, cystic, fatty and calcific components possible. Regarding intra-abdominal tumors, most are sacrococcygeal teratomas. Yolk sac tumor is the malignant germ cell tumor most likely to occur in the perinatal period, and this adversely impacts prognosis. It can occur alone or with a teratoma and is most commonly seen with sacrococcygeal teratomas (10%) [55]. More commonly, poor prognosis for fetal sacrococcygeal teratomas is related to vascular shunting, hydrops and mass effect. Sacrococcygeal teratomas make up 40% of all fetal teratomas [55]. There are case reports of purely abdominal teratomas, usually arising from the gonads, specifically in undescended testes in the fetus [56–60]. Perinatal gastric, retroperitoneal, liver and ileum teratomas have been reported in the pathology literature [55].

Fetus in fetu

Teratoma can be differentiated from fetus in fetu by the presence of a vertebral column in the latter, and some argue that limbs should be present as well [61]. Fetus in fetu is most commonly found in the retroperitoneum.

Abdominal cysts

Any abdominal cyst has the potential to hemorrhage and appear complex, mimicking a solid mass. Meconium peritonitis and meconium pseudocyst sometimes mimic a solid mass because of their complexity. T1-W hyperintense signal on MRI helps to differentiate hemorrhage and meconium from solid tumors. Also, some mass lesions are mixed solid and cystic, particularly mesenchymal hamartoma and cystic neuroblastoma. Although a detailed review of cystic abdominal

Table 4 Differential diagnoses of cystic fetal abdominal masses, which can mimic a solid mass if complex, based on location

Right upper quadrant	Left upper quadrant	Mid-abdomen	Retroperitoneal	Low abdomen/ pelvis	Any location
Choledochal cyst	Splenic cyst	Lymphatic cyst	Urinary tract dilation	Ovarian cyst	Alimentary duplication cyst
Hepatic cyst	Gastric duplication cyst	Meconium pseudocyst	Cystic renal disease	Hydrometrocolpos	Dilated bowel
Duodenal duplication cyst	Pancreatic tail cyst	Pancreatic body cyst	Urinoma	Ureterocele	Cystic teratoma
Duodenal atresia/stenosis			Adrenal cyst	Urachal cyst	
Gallbladder duplication			Lymphatic cyst	Megacystis	
Pancreatic head cyst				Cloaca	
				Anterior sacral meningocele	
				Sacrococcygeal teratoma	

masses is beyond the scope of this paper, Table 4 lists the differential diagnoses of fetal cystic masses based on location in the abdomen. The more commonly encountered fetal abdominal cysts include ovarian cyst, urinary tract dilation, multicystic dysplastic kidney, choledochal cyst, bowel dilation, enteric duplication cyst, and lymphatic cyst (including mesenteric, omental and retroperitoneal) [62].

Ovarian tumor

Ovarian cysts are common, but there are rare reports of ovarian malignancies that have a solid component and are present in the abdomen [63]. Ovarian torsion, with or without a cyst, might also present as a complex abdominal or pelvic prenatal mass in a female [64].

Conclusion

Solid fetal or perinatal abdominal tumors are rare and are identified in the second and third trimesters. All abdominal tumors are at risk for mass effect resulting in cardiopulmonary compromise from vascular compression and pulmonary hypoplasia or gastrointestinal obstruction, so serial US imaging during pregnancy should be performed to monitor for complications. Large masses can also predispose to abdominal dystocia and impact decisions regarding cesarean section, though the decision is largely based on obstetric indications because there are no evidence-based guidelines regarding abdominal circumference or tumor size [1, 23, 25].

The most common primary fetal liver tumors include hemangioma, mesenchymal hamartoma and hepatoblastoma. Mesenchymal hamartoma is predominantly cystic, and hemangioma and hepatoblastoma are predominantly solid. Rapid growth supports a malignant hepatoblastoma diagnosis. Postnatal enhancement pattern is useful to confirm the diagnosis, and serum alpha-fetoprotein is not useful to diagnose hepatoblastoma.

The most common renal tumors include congenital mesoblastic nephroma, Wilms tumor, malignant rhabdoid tumor of the kidney, and clear cell sarcoma of the kidney. MRI is useful to look for clues to re-order the differential diagnosis, but nephrectomy and pathology are diagnostic. Renal tumors put fetuses particularly at risk for polyhydramnios and preterm labor. Postnatal MRI or CT and staging should be performed preoperatively.

The differential diagnosis for a suprarenal mass includes neuroblastoma, adrenal hemorrhage and subdiaphragmatic extralobar sequestration. Neuroblastoma and adrenal hemorrhage tend to be on the right side and sequestration on the left. Neuroblastoma and hemorrhage involve the adrenal gland and might appear cystic, solid or mixed. MRI signal, presence of metastases, and follow-up over time differentiate neuroblastoma from hemorrhage. Subdiaphragmatic extralobar sequestration is separate from the adrenal gland and spine, is more homogeneous and T2-hyperintense than neuroblastoma, and might be associated with a diaphragm defect. The diagnosis is typically narrowed reliably prenatally, so that only US follow-up is performed unless neuroblastoma is the prenatal diagnosis.

A systematic approach including US and MRI to identify the organ of origin and imaging characteristics narrow the differential diagnosis.

Compliance with ethical standards

Conflicts of interest None

References

1. Amari F, Beyer DA, Diedrich K, Weichert J (2013) Fetal intra-abdominal tumors: assessment of spectrum, accuracy of prenatal

diagnosis, perinatal outcome and therapy at a tertiary referral center. Eur J Obstet Gynecol Reprod Biol 167:160–166
2. Isaacs H (2007) Fetal and neonatal hepatic tumors. J Pediatr Surg 42:1797–1803
3. Marks F, Thomas P, Lustig I et al (1990) In utero sonographic description of a fetal liver adenoma. J Ultrasound Med 9:119–122
4. Applegate KE, Ghei M, Perez-Atayde AR (1999) Prenatal detection of a solitary liver adenoma. Pediatr Radiol 29:92–94
5. Petrikovsky BM, Cohen HL, Scimeca P, Bellucci E (1994) Prenatal diagnosis of focal nodular hyperplasia of the liver. Prenat Diagn 14: 406–409
6. Demir HA, Varan A, Akçören Z et al (2008) Focal nodular hyperplasia of the liver and elevated alpha fetoprotein level in an infant with isolated hemihyperplasia. J Pediatr Hematol Oncol 30:775–777
7. International Society for the Study of Vascular Anomalies (2014) ISSVA classification of vascular anomalies. http://issva.org/classification. Accessed 22 Jan 2019
8. Mo JQ, Dimashkieh HH, Bove KE (2004) GLUT1 endothelial reactivity distinguishes hepatic infantile hemangioma from congenital hepatic vascular malformation with associated capillary proliferation. Hum Pathol 35:200–209
9. Johnson CM, Navarro OM (2017) Clinical and sonographic features of pediatric soft-tissue vascular anomalies Part 1: classification, sonographic approach and vascular tumors. Pediatr Radiol 47: 1184–1195
10. Merrow AC, Gupta A, Patel MN, Adams DM (2016) 2014 revised classification of vascular lesions from the International Society for the Study of Vascular Anomalies: radiologic-pathologic update. Radiographics 36:1494–1516
11. Christison-Lagay ER, Burrows PE, Alomari A et al (2007) Hepatic hemangiomas: subtype classification and development of a clinical practice algorithm and registry. J Pediatr Surg 42:62–67
12. Kulungowski AM, Alomari AI, Chawla A et al (2012) Lessons from a liver hemangioma registry: subtype classification. J Pediatr Surg 47:165–170
13. Ackermann O, Fabre M, Franchi S et al (2011) Widening spectrum of liver angiosarcoma in children. J Pediatr Gastroenterol Nutr 53: 615–619
14. Stringer MD, Alizai NK (2005) Mesenchymal hamartoma of the liver: a systematic review. J Pediatr Surg 40:1681–1690
15. Cornette J, Festen S, van den Hoonaard TL, Steegers EAP (2009) Mesenchymal hamartoma of the liver: a benign tumor with deceptive prognosis in the perinatal period. Case report and review of the literature. Fetal Diagn Ther 25:196–202
16. Spector LG, Birch J (2012) The epidemiology of hepatoblastoma. Pediatr Blood Cancer 59:776–779
17. Herzog CE, Andrassy RJ, Eftekhari F (2000) Childhood cancers: hepatoblastoma. Oncologist 5:445–453
18. Trobaugh-Lotrario AD, Chaiyachati BH, Meyers RL et al (2013) Outcomes for patients with congenital hepatoblastoma. Pediatr Blood Cancer 60:1817–1825
19. Isaacs H (2008) Fetal and neonatal renal tumors. J Pediatr Surg 43: 1587–1595
20. Patil PS, Gupta A, Gupta R et al (2017) Unusual presentation of metanephric stromal tumor in a neonate. Indian J Med Paediatr Oncol 38:357–359
21. Gedikbasi A, Oztarhan K, Ulker V et al (2011) Prenatal sonographic diagnosis of tuberous sclerosis complex. J Clin Ultrasound JCU 39:427–430
22. Linam LE, Yu X, Calvo-Garcia MA et al (2010) Contribution of magnetic resonance imaging to prenatal differential diagnosis of renal tumors: report of two cases and review of the literature. Fetal Diagn Ther 28:100–108
23. Leclair M-D, El-Ghoneimi A, Audry G et al (2005) The outcome of prenatally diagnosed renal tumors. J Urol 173:186–189
24. van den Heuvel-Eibrink MM, Grundy P, Graf N et al (2008) Characteristics and survival of 750 children diagnosed with a renal tumor in the first seven months of life: a collaborative study by the SIOP/GPOH/SFOP, NWTSG, and UKCCSG Wilms tumor study groups. Pediatr Blood Cancer 50:1130–1134
25. Berger M, von Schweinitz D (2015) Current management of fetal and neonatal renal tumors. Curr Pediatr Rev 11:188–194
26. Powis M (2010) Neonatal renal tumours. Early Hum Dev 86:607–612
27. Suresh I, Suresh S, Arumugam R et al (1997) Antenatal diagnosis of Wilms tumor. J Ultrasound Med 16:69–72
28. Ritchey ML, Azizkhan RG, Beckwith JB et al (1995) Neonatal Wilms tumor. J Pediatr Surg 30:856–859
29. Chung CJ, Cammoun D, Munden M (1990) Rhabdoid tumor of the kidney presenting as an abdominal mass in a newborn. Pediatr Radiol 20:562–563
30. Stanescu AL, Acharya PT, Lee EY, Phillips GS (2019) Pediatric renal neoplasms: MR imaging-based practical diagnostic approach. Magn Reson Imaging Clin N Am 27:279–290
31. Gooskens SLM, Furtwängler R, Vujanic GM et al (2012) Clear cell sarcoma of the kidney: a review. Eur J Cancer 48:2219–2226
32. Furtwängler R, Gooskens SL, van Tinteren H et al (2013) Clear cell sarcomas of the kidney registered on International Society of Pediatric Oncology (SIOP) 93-01 and SIOP 2001 protocols: a report of the SIOP renal tumour study group. Eur J Cancer 49:3497–3506
33. Sherer DM, Dalloul M, Wagreich A et al (2008) Prenatal sonographic findings of congenital adrenal cortical adenoma. J Ultrasound Med 27:1091–1093
34. Sarwar ZU, Ward VL, Mooney DP et al (2004) Congenital adrenocortical adenoma: case report and review of literature. Pediatr Radiol 34:991–994
35. Izbizky G, Elias D, Gallo A et al (2005) Prenatal diagnosis of fetal bilateral adrenal carcinoma. Ultrasound Obstet Gynecol 26:669–671
36. Chen CP, Chen SH, Chuang CY et al (1997) Clinical and perinatal sonographic features of congenital adrenal cystic neuroblastoma: a case report with review of the literature. Ultrasound Obstet Gynecol 10:68–73
37. Gali S, Anat I (2015) Purely cystic adrenal lesion in a newborn evolving into a solid neuroblastoma. J Clin Ultrasound 43:126–128
38. Isaacs H (2007) Fetal and neonatal neuroblastoma: retrospective review of 271 cases. Fetal Pediatr Pathol 26:177–184
39. Desai G, Filly RA, Rand L (2009) Prenatal detection of an extra-adrenal neuroblastoma with hepatic metastases. J Ultrasound Med 28:1085–1090
40. Curtis MR, Mooney DP, Vaccaro TJ et al (1997) Prenatal ultrasound characterization of the suprarenal mass: distinction between neuroblastoma and subdiaphragmatic extralobar pulmonary sequestration. J Ultrasound Med 16:75–83
41. Eo H, Kim JH, Jang KM et al (2011) Comparison of clinicoradiological features between congenital cystic neuroblastoma and neonatal adrenal hemorrhagic pseudocyst. Korean J Radiol 12:52–58
42. Hwang SM, Yoo S-Y, Kim JH, Jeon TY (2016) Congenital adrenal neuroblastoma with and without cystic change: differentiating features with an emphasis on the of value of ultrasound. AJR Am J Roentgenol 207:1105–1111
43. Flanagan SM, Rubesova E, Jaramillo D, Barth RA (2016) Fetal suprarenal masses — assessing the complementary role of magnetic resonance and ultrasound for diagnosis. Pediatr Radiol 46:246–254
44. Brodeur GM (2018) Spontaneous regression of neuroblastoma. Cell Tissue Res 372:277–286
45. Heling KS, Chaoui R, Hartung J et al (1999) Prenatal diagnosis of congenital neuroblastoma. Analysis of 4 cases and review of the literature. Fetal Diagn Ther 14:47–52

46. Gyurkovits Z, Maróti Á, Rénes L et al (2015) Adrenal haemorrhage in term neonates: a retrospective study from the period 2001–2013. J Matern Fetal Neonatal Med 28:2062–2065
47. Lee MC, Lin LH (2000) Ultrasound screening of neonatal adrenal hemorrhage. Acta Paediatr Taiwanica 41:327–330
48. Toti MS, Ghirri P, Bartoli A et al (2019) Adrenal hemorrhage in newborn: how, when and why — from case report to literature review. Ital J Pediatr 45:58
49. Riley JS, Urwin JW, Oliver ER et al (2018) Prenatal growth characteristics and pre/postnatal management of bronchopulmonary sequestrations. J Pediatr Surg 53:265–269
50. Zhang N, Zeng Q, Chen C et al (2019) Distribution, diagnosis, and treatment of pulmonary sequestration: report of 208 cases. J Pediatr Surg 54:1286–1292
51. Dhingsa R, Coakley FV, Albanese CT et al (2003) Prenatal sonography and MR imaging of pulmonary sequestration. AJR Am J Roentgenol 180:433–437
52. Obeidat N, Sallout B, Alaali W (2016) Isolated subdiaphragmatic extralobar pulmonary sequestration: masquerading as suprarenal mass with spontaneous resolution. Clin Exp Obstet Gynecol 43: 457–459
53. Adzick NS, Harrison MR, Crombleholme TM et al (1998) Fetal lung lesions: management and outcome. Am J Obstet Gynecol 179: 884–889
54. Laberge J-M, Puligandla P, Flageole H (2005) Asymptomatic congenital lung malformations. Semin Pediatr Surg 14:16–33
55. Isaacs H (2004) Perinatal (fetal and neonatal) germ cell tumors. J Pediatr Surg 39:1003–1013
56. Janda GM, Najdzionek JS, Kozielski R et al (2014) Early prenatal detection of an intra-abdominal cryptorchid testicular teratoma. Urology 83:214–216
57. Youssef A, Salsi G, Curti A et al (2016) Prenatal ultrasonographic features of mature cystic teratoma in undescended testicle. Ultrasound Obstet Gynecol 47:527–529
58. Siu SS, Leung TN, Leung TY et al (2001) Prenatal diagnosis of intra-abdominal mature testicular teratoma. J Ultrasound Med 20: 1257–1260
59. Shih HH, Teng RJ, Yau KI et al (1997) Mature teratoma arising from an intra-abdominal undescended testis presenting as a fetal abdominal mass. Ultrasound Obstet Gynecol 10:209–211
60. Wagner N, Kagan KO, Warmann SW et al (2009) Prenatal diagnosis and management of a fetal intra-abdominal teratoma: a case report and review of the literature. Fetal Diagn Ther 26:170–172
61. Basu A, Jagdish S, Iyengar KR, Basu D (2006) Fetus in fetu or differentiated teratomas? Indian J Pathol Microbiol 49:563–565
62. Birkemeier K (2015) Abdominal masses. In: Kline-Fath B, Bulas D, Bahadho-Singh R (eds) Fundamental and advanced fetal imaging. Wolters Kluwer Health, Philadelphia, pp 651–659
63. Dimitraki M, Koutlaki N, Nikas I et al (2012) Fetal ovarian cysts. Our clinical experience over 16 cases and review of the literature. J Matern Fetal Neonatal Med 25:222–225
64. Ozcan HN, Balci S, Ekinci S et al (2015) Imaging findings of fetal-neonatal ovarian cysts complicated with ovarian torsion and autoamputation. AJR Am J Roentgenol 205:185–189